

## Direct numerical simulations of premixed and stratified flame propagation in turbulent channel flow

Andrea Gruber\*

*SINTEF Energy Research, Thermal Energy Department, 7465 Trondheim, Norway  
and Norwegian University of Science and Technology, Department of Energy and Process Engineering,  
7491 Trondheim, Norway*

Edward S. Richardson

*University of Southampton, SO17 1BJ Southampton, United Kingdom*

Konduri Aditya and Jacqueline H. Chen

*Sandia National Laboratories, Livermore, California 94550, USA*



(Received 16 August 2018; published xxxxxx)

Direct numerical simulations are performed to investigate the transient upstream flame propagation (flashback) through homogeneous and fuel-stratified hydrogen-air mixtures transported in fully developed turbulent channel flows. Results indicate that, for both cases, the flame maintains steady propagation against the bulk flow direction, and the global flame shape and the local flame characteristics are both affected by the occurrence of fuel stratification. Globally, the mean flame shape undergoes an abrupt change when the approaching reactants transition from an homogeneous to a stratified mixing configuration. A V-shaped flame surface, whose leading-edge is located in the near-wall region, characterizes the nonstratified, homogeneous mixture case, while a U-shaped flame surface, whose leading edge propagates upstream at the channel centerline, distinguishes the case with fuel stratification (fuel-lean in the near-wall region and fuel-rich away from the wall). The characteristic thickness, wrinkling, and displacement speed of the turbulent flame brush are subject to considerable changes across the channel due to the dependence of the turbulence and mixture properties on the distance from the channel walls. More specifically, the flame transitions from a moderately wrinkled, thin-flamelet combustion regime in the homogeneous mixture case to a strongly wrinkled flame brush more representative of a thickened-flame combustion regime in the near-wall region of the fuel-stratified case. The combustion regime may be related to the Karlovitz number, and it is shown that a *nominal* channel-flow Karlovitz number,  $Ka_{in}^{ch}$ , based on the wall-normal variation of canonical turbulence ( $t_\eta = (\nu/\epsilon)^{1/2}$ ) and chemistry ( $t_l = \delta_l/S_l$ ) timescales in fully developed channel flow, compares well with an *effective* Karlovitz number,  $Ka_n^{ch}$ , extracted from the present DNS datasets using conditionally sampled values of  $t_\eta$  and  $t_l$  in the immediate vicinity of the flame ( $0.1 < C < 0.3$ ).

DOI: [10.1103/PhysRevFluids.00.000500](https://doi.org/10.1103/PhysRevFluids.00.000500)

### I. INTRODUCTION

#### A. Background and motivation

The process of unsteady flame propagation in turbulent, confined flows is of great importance for many industrial applications. State-of-the-art gas turbine combustors, scramjets, and, generally,

\*andrea.gruber@sintef.no

many recent internal combustion engines operate, more often than in the past, at increasingly high-power densities that result in relatively large surface-to-volume ratios for the combustion chamber. The practical implementation of this trend is typically accompanied by the common occurrence of reactive flows where the flame is anchored or freely propagates in confined ducts, channels, or vessels whose size is increasingly small relative to the size of the flame. If operated in a premixed fashion, such combustion systems are likely to be operated on the border of the stable flame region [1] and are often subject to thermoacoustic instabilities, flame blow-out, or flashback. Flashback is characterized by unsteady often abrupt and rapid flame propagation upstream of the flame's design position into the premixing section of the burner, and understanding this process is the objective of the present study.

It is well-known that flashback is characterized by a number of different initiating mechanisms [2]. Flashback that occurs near the burner walls in the boundary layer of the flow is known as boundary layer flashback and is a safety issue for nonconventional and highly reactive fuels containing hydrogen. A recent comprehensive review [3] summarizes the status of knowledge on the physical mechanism behind boundary layer flashback in nonswirling flows, highlighting the challenges presented by the eventual adoption of fuels with increased reactivity. The addition of even small quantities of hydrogen to less reactive hydrocarbon fuels can alter the reactivity of these fuels in a drastic nonlinear fashion [4,5]. The reason for this is due to the specific combustion characteristics of hydrogen, recently summarized by Sanchez and Williams [6], that ultimately reduce the flame-quenching distance [7], and therefore is able to support relatively high flame speed in the low-velocity region of the flow very close to the wall. Accordingly, the adoption of hydrogen-containing fuels introduces a number of design issues in state-of-the-art gas turbines [8] where the occurrence of the flame flashback process is often complicated further by the swirling pattern of the underlying turbulent flow. See Refs. [9,10] for a recent excellent experimental characterization of flashback in swirling flows.

A practical design feature in gas turbine burners that considerably complicates the understanding of unsteady flame propagation during flashback is the presence of fuel-oxidant stratification and partial premixing. Here, the term *partially premixing* refers to compositionally inhomogeneous mixtures that include flammable and nonflammable fluid, while *stratification* refers to a reacting front propagating through a mixture containing a range of compositions within the flammability limits [11]. Once flashback is initiated and the flame propagates upstream into the mixing section of the burner, the flame encounters a progressively less homogeneous flow of reactants, either temporarily, as a consequence of a transient perturbation of the fuel delivery system flow rate, or permanently, as the flame establishes itself within the premixer section of the burner. In fact, it is reasonable to assume that, during a typical flashback event, flame propagation begins in conditions of *premixed combustion* at the flame design position, first evolving toward a *stratified combustion* situation, followed by propagation in *partially premixed* conditions that eventually leads to extinction or, if the flame survives, to *nonpremixed combustion* if the flame anchors directly at the fuel injection nozzles according to the flame-flow interaction mechanism that characterizes transverse jets [12–15]. It is also important to mention that, in modern low-emissions industrial burners, some degree of unmixedness, occurring either as partially premixed reactants or as fuel-oxidant stratification, is often an intentional design feature, even at the flame design position, to achieve good flame stability properties [16]. For these reasons, the present work aims to achieve accurate insight and good understanding of flame propagation behavior in confined flows of reactants that are characterized by a spatial variation of the reactant composition within the flammability limits (stratification).

## B. Previous work on boundary layer flashback

The seminal paper by Lewis and von Elbe [17] is the first study to systematically investigate flashback limits and has remained as the state-of-the-art for order-of-magnitude flashback prediction. However, this pioneering model from 1943, in determining the critical velocity gradient for

the onset of flashback, erroneously assumes that the premixed flame propagating along the wall boundary layer has no effect on the approaching flow of reactants. In the past, practical difficulties in performing accurate experimental measurements in the near-wall region of reactive flows have represented a considerable challenge and only recently improved laser-based diagnostic techniques have enabled the acquisition of high-quality empirical data on flame-wall interactions [18] and near-wall flame propagation [19]. Recent experimental and numerical investigations of swirling and nonswirling reactive flows [10,19–21] have revealed the presence of flame-induced flow reversals in the viscous layer ( $y^+ \lesssim 20$ ) immediately upstream of the flame surface. These flow reversal “pockets” are consistently associated with regions of the flame front that are convex toward the reactants. In nonswirling flows, the convex leading-edge “bulges” of the flame front are, in turn, clearly correlated with the low-velocity streaks of the turbulent boundary layer [21]. These recent findings provide a radically different picture of the mechanism of boundary layer flashback and also underscores the need for near-wall flame propagation models that correctly accounts for this new conceptual understanding [22–24].

Early studies on flashback, building on the methodology proposed in Ref. [17], tried to chart the flashback behavior of premixed flames in the transition from laminar flow to the more interesting case of turbulent flow and empirical observations showed a considerable increase of the critical velocity gradient in the presence of turbulence [25,26]. This increase is consistent with the interpretation of the flashback mechanism for turbulent flames provided in Ref. [21] that highlights the limitations of a flashback theory ultimately based on a velocity balance within the quasi-laminar viscous layer. More recent modeling studies [27–29] have taken into account local Lewis number and flame curvature effects on the onset of laminar boundary layer flashback. However, these analyses often consider flame surface curvature and displacement speed effects only by taking into account the wall-normal direction and therefore are restricted by the assumption that boundary layer flashback is governed by physical processes whose main characteristics are two-dimensional.

The recent direct numerical simulations (DNS) performed by the present research group suggest that three-dimensional effects play a fundamental role in turbulent flame-wall interactions in general [30] and in the physical mechanism behind boundary layer flashback in particular [21,22]. The presence in the fresh reactants of relatively low-velocity fluid organized in thin, elongated streaky regions, very close to the wall, provides ideal “trails” along which flame tongues at the front’s leading-edge can advance, “slipping” underneath the bulk flow, to achieve upstream propagation during flashback. The three-dimensional nature of this process has a central role: even if the velocity gradient at the wall associated with the turbulent boundary layer is, in the mean, above the critical value for flashback to occur, the flame front can still encounter, locally, wall velocity gradients well below the critical value within the low-velocity streaky regions, ultimately resulting in leading point flame propagation.

The conceptual picture drawn above highlights the key role that spatial and temporal variations in fluid momentum play in near-wall flame propagation, but it does not consider the effect of variations in the fluid’s composition and reactivity. These too are expected to affect the competition between fluid velocity and flame surface displacement speed, and to affect the flame propagation characteristics, both locally and globally.

Stratified combustion has been the subject of numerous modeling and experimental studies in recent years and the interested reader is advised to examine the careful review by Masri [11]. Most fundamental experimental studies of turbulent stratified combustion have considered unconfined flow configurations, for example free shear flows with different fuel/air blends introduced through concentric tubes. A few laboratory studies have examined stratification effects in small technical burners, as a model for combustion processes found in gas turbine combustors. However, none of these studies about stratified combustion have specifically considered confined flame propagation in ducts or channel configurations that would allow for a detailed investigation of flame-wall interactions and flashback.

The objective of the present study is to investigate unsteady propagation of a stratified flame during a flashback event that occurs in fully developed turbulent channel flow. This configuration is

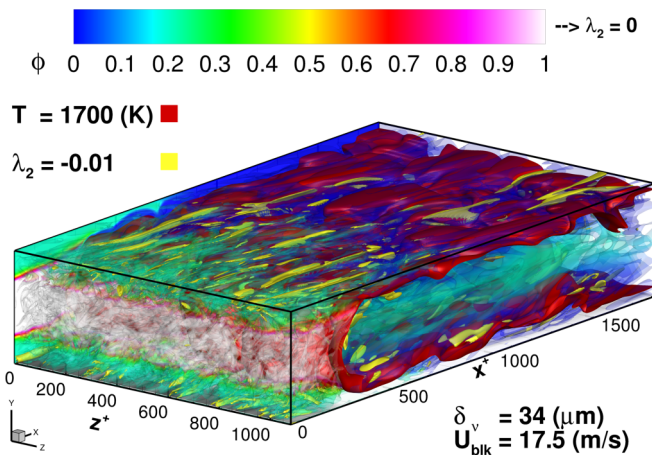


FIG. 1. Upstream flame propagation during flashback in a stratified mixture: the red surface demarcates a fluid temperature of  $T = 1700$  (K) while the channel-flow turbulence is visualized using the second eigenvalue of the vorticity gradient tensor,  $\lambda_2$ . The nontranslucent yellow isosurfaces correspond to relatively strong vorticity within the near-wall coherent structures of the boundary layer,  $\lambda_2 = -0.01$ , while the local equivalence ratio is represented using the color scale shown using transparency on the  $\lambda_2 = 0.0$  isosurfaces.

144 similar to the one adopted in Ref. [21]; however, in the new case considered here, a compositional  
 145 inhomogeneity is introduced at the channel inlet: specifically, fuel-lean conditions are imposed  
 146 in the near-wall regions while the mixture is fuel-rich in the bulk flow around the channel  
 147 centerline. After the initial transition from premixed to stratified combustion, the compositional  
 148 stratification introduced here ultimately results in a turbulent flame steadily propagating upstream  
 149 against the bulk flow direction with the leading-edge at the channel centerline; see Fig. 1. This  
 150 new DNS database enables a detailed comparison versus the premixed cases already discussed in  
 151 Refs. [21,22]. Accordingly, the present DNS builds upon and complements the earlier DNS and  
 152 high-resolution experimental studies [19,21,22,30–33] that were also conducted in the framework  
 153 of the BIGCO2/BIGCCS R&D platforms.

154 The remainder of this paper is organized as follows: the DNS code and the problem formulation  
 155 are described in Sec. II. A comprehensive analysis of the DNS results from the new stratified mixture  
 156 case along with a comparison with earlier results from the homogeneous mixture case are presented  
 157 in Sec. III. Finally, conclusions and recommendations for further work are presented in Sec. IV.

## 158 II. MATHEMATICAL FORMULATION, CASE CONFIGURATION, AND DNS CODE

159 The Navier-Stokes equations in their compressible formulation are solved in a three-dimensional  
 160 computational domain to simulate the upstream propagation of nonanchored, premixed, and  
 161 stratified  $H_2$ -air flames in fully developed turbulent channel flow at a pressure of 2 (atm) and at  
 162 a global equivalence ratio varying between  $\phi \sim 0.55$  (stationary value) and  $\phi \sim 0.7$  (peak transient  
 163 value). We shall refer to the three spatial directions in the computational domain as: streamwise  
 164 direction ( $x$ ), wall-normal direction ( $y$ ), and spanwise direction ( $z$ ). In the comparison reported  
 165 below, the earlier premixed case and the present stratified case are denoted as TCF055<sub>h</sub> and  
 166 TCF055<sub>s</sub>, respectively, and these subscripts are used consistently in the remainder of the present  
 167 paper.

168 Thermodynamic properties are modeled as polynomial functions of temperature and transport  
 169 coefficients as described in the CHEMKIN and TRANSPORT packages, respectively [34]. Radiative  
 170 heat transfer is not considered in this study and the temperature of the walls and of the reactants  
 171 is set to 750 (K) for both TCF055<sub>h</sub> and TCF055<sub>s</sub>. The chemical reactions in the gas phase are

TABLE I. The complete 9-species, 19-reactions hydrogen-air chemical kinetics mechanism from Ref. [35].

$n$	Reaction	B	$a$	$E_a$
1	$\text{O}_2 + \text{H} \rightleftharpoons \text{OH} + \text{O}$	$3.547 \times 10^{15}$	-0.406	$1.6599 \times 10^4$
2	$\text{H}_2 + \text{O} \rightleftharpoons \text{OH} + \text{H}$	$0.508 \times 10^5$	2.67	$0.629 \times 10^4$
3	$\text{OH} + \text{H}_2 \rightleftharpoons \text{H} + \text{H}_2\text{O}$	$0.216 \times 10^9$	1.51	$0.343 \times 10^4$
4	$\text{H}_2\text{O} + \text{O} \rightleftharpoons 2\text{OH}$	$2.97 \times 10^6$	2.02	$1.34 \times 10^4$
5	$\text{H}_2 + \text{M} \rightleftharpoons 2\text{H} + \text{M}$	$4.577 \times 10^{19}$	-1.40	$1.0438 \times 10^5$
6	$2\text{O} + \text{M} \rightleftharpoons \text{O}_2 + \text{M}$	$6.165 \times 10^{15}$	-0.50	0.0
7	$\text{H} + \text{O} + \text{M} \rightleftharpoons \text{OH} + \text{M}$	$4.714 \times 10^{18}$	-1.00	0.0
8	$\text{OH} + \text{H} + \text{M} \rightleftharpoons \text{H}_2\text{O} + \text{M}$	$3.800 \times 10^{22}$	-2.00	0.0
9	$\text{O}_2 + \text{H}(+\text{M}) \rightleftharpoons \text{HO}_2(+\text{M})$	$1.475 \times 10^{12}$	0.60	0.0
10	$\text{H} + \text{HO}_2 \rightleftharpoons \text{O}_2 + \text{H}_2$	$1.66 \times 10^{13}$	0.00	$0.823 \times 10^3$
11	$\text{H} + \text{HO}_2 \rightleftharpoons 2\text{OH}$	$7.079 \times 10^{13}$	0.00	$2.95 \times 10^2$
12	$\text{O} + \text{HO}_2 \rightleftharpoons \text{OH} + \text{O}_2$	$0.325 \times 10^{14}$	0.00	0.0
13	$\text{OH} + \text{HO}_2 \rightleftharpoons \text{O}_2 + \text{H}_2\text{O}$	$2.890 \times 10^{13}$	0.00	$-4.970 \times 10^2$
14	$2\text{HO}_2 \rightleftharpoons \text{O}_2 + \text{H}_2\text{O}_2$	$4.200 \times 10^{14}$	0.00	$1.1982 \times 10^4$
15	$\text{H}_2\text{O}_2(+\text{M}) \rightleftharpoons 2\text{OH}(+\text{M})$	$2.951 \times 10^{14}$	0.00	$4.843 \times 10^4$
16	$\text{H} + \text{H}_2\text{O}_2 \rightleftharpoons \text{OH} + \text{H}_2\text{O}$	$0.241 \times 10^{14}$	0.00	$0.397 \times 10^4$
17	$\text{H} + \text{H}_2\text{O}_2 \rightleftharpoons \text{H}_2 + \text{HO}_2$	$0.482 \times 10^{14}$	0.00	$0.795 \times 10^4$
18	$\text{O} + \text{H}_2\text{O}_2 \rightleftharpoons \text{HO}_2 + \text{OH}$	$9.550 \times 10^6$	2.00	$3.970 \times 10^3$
19	$\text{OH} + \text{H}_2\text{O}_2 \rightleftharpoons \text{H}_2\text{O} + \text{HO}_2$	$5.800 \times 10^{14}$	0.00	$9.557 \times 10^3$

described by a detailed mechanism for hydrogen combustion in air [35]. This mechanism consists of 9 species and 19 elementary reaction steps; see Table I for details. Nitrogen is assumed to be inert such that  $\text{NO}_x$ -formation reactions are not considered. The stratification of the reactant mixture entering the channel is introduced by imposing, at the domain inlet ( $x = 0$ ), a spatial variation of the local equivalence ratio that is smoothly adjusted between a fuel-lean value of  $\phi \sim 0.2$  in the near-wall region and a fuel-rich value of  $\phi \sim 1.2$  in the bulk flow; see Fig. 2.

The Reynolds number of the approach flow is  $\text{Re}_0 \sim 3200$  for both cases considered here, based on the channel mean centerline velocity  $U_c^f$  of the fresh reactants and the channel half-width  $h$ . This corresponds to a friction Reynolds number,  $\text{Re}_\tau \sim h/\delta_\nu \sim 180$ , where  $\delta_\nu$  is the viscous length scale.

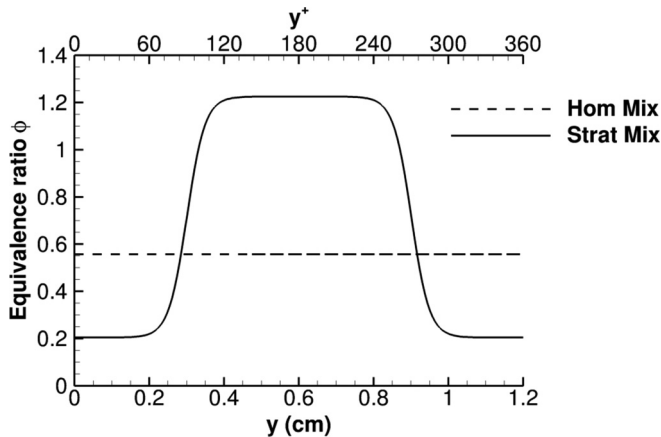


FIG. 2. Profile of equivalence ratio ( $\phi$ ) versus wall-distance in dimensional ( $y$ ) and nondimensional form ( $y^+$ ) illustrating the imposed spatial variation in mixture composition at the domain inlet,  $x = 0$ .

TABLE II. Physical parameters for the simulated reactive cases:  $\phi_w$  is the near-wall equivalence ratio,  $h$  the channel half-width,  $\delta_v$  the viscous length scale and  $Da^w$  the Damköhler number that describes the near-wall combustion regime.

Case name	$\phi_w$	$U_c^f$	$h$	$L_x \times L_y \times L_z$	$\delta_v$	$S_l/U_c^f$	$Da^w$	convective transit time (effective)
TCF055h	0.55	20 (m/s)	6 (mm)	$10h \times 2h \times 6h$	$3.4 \times 10^{-05}$ (m)	0.35	0.69	1.5 (ms)
TCF055s	0.20– 1.20	20 (m/s)	6 (mm)	$10h \times 2h \times 6h$	$3.4 \times 10^{-05}$ (m)	0.059– 0.65	0.06– 0.85	1.5 (ms)

All turbulent quantities used below for nondimensionalization characterize the turbulent flow of the fresh reactants upstream of the flame. The *wall Damköhler number*  $Da^w$  is the ratio of turbulent and chemical timescales that characterizes the combustion regime of turbulent flames in the near-wall regions of the flow. The conditions simulated give  $Da_h^w \sim 0.69$  and  $Da_s^w \sim 0.06$  for the premixed and stratified cases, respectively. As suggested in Ref. [30], these wall Damköhler numbers  $Da^w$  are based on the freely propagating one-dimensional laminar flame timescale [ $t_{lh} = \delta_{lh}/S_{lh} \sim 4.8 \times 10^{-05}$  (s) and  $t_{ls} = \delta_{ls}/S_{ls} \sim 5.3 \times 10^{-04}$  (s)] and on the wall timescale that is uniquely defined from the turbulent channel flow of the fresh reactants [ $t_{wh} = t_{ws} = \nu/u_\tau^2 \sim 3.3 \times 10^{-05}$  (s)]. In these expressions  $u_\tau$  is the friction velocity,  $\nu$  is the kinematic viscosity of the fresh reactants, and  $\delta_{lh,s}$  and  $S_{lh,s}$  are the laminar flame thickness and laminar flame velocities for the equivalence ratios present in the near-wall regions for the premixed and stratified case indicated by subscript  $h$  and  $s$ , respectively. It should be noted that the flame thickness,  $\delta_{lh,s}$ , at  $\phi = 0.55$  and  $\phi = 0.2$ , respectively are estimated in terms of the fuel reaction rate thickness. Other relevant parameters of the DNS are given in Table II. Note that the nondimensional mean centerline velocity is  $u_c^+ \sim U_c^f/u_\tau \sim 19$  and channel bulk velocity is  $U_{blk} = 17.5$  (m/s).

The turbulent  $H_2$ -air mixture, with a fuel mass flow rate of approximately  $\sim 0.1$  (g/s) for both the premixed and the stratified case, enters the channel from a partially nonreflecting inflow boundary at  $x = 0$  and approaches the flame in the streamwise direction while the burnt products leave the computational domain from a partially nonreflecting outflow boundary at  $x = L_x$ . Inflow and outflow boundary conditions are implemented following the Navier-Stokes characteristic boundary conditions (NSCBC) methodology and are based on the original formulation of Ref. [36], incorporating the later improvements described in Refs. [37–39] that include source and transverse terms. No-slip isothermal wall boundaries ( $y = 0$  and  $y = L_y$ ) are implemented following the methodology described in Refs. [33,40] for solid (nonporous) surfaces. Periodic (cyclic) boundary conditions are adopted in the spanwise direction ( $z = 0$  and  $z = L_z$ ), which results in statistical homogeneity in the  $z$  direction, providing increased sample size for statistical analysis and averaging. The wall is assumed to be impermeable, so the wall-normal mass flux of all chemical species is set to zero.

The three-dimensional Cartesian grid is uniform in all directions. The first point from the wall is at  $y^+ = 0.73$ , where the superscript + indicates nondimensionalization by the viscous length scale. There are 13 points within  $y^+ = 10$  to satisfy the resolution requirements in the viscous layer [41]. The grid resolution is  $\Delta x^+ = \Delta y^+ = \Delta z^+ = 0.73$  (equivalent to  $25 \mu\text{m}$ ) in both the premixed and the stratified case. The grid is not stretched, not even in the wall-normal direction, to accurately represent the flame which requires high spatial resolution throughout the channel, including near the centerline. See Table III for an overview of the DNS parameters.

### A. Initialization and transition from premixed to stratified combustion

The reactive, premixed case is initialized using an auxiliary nonreacting flow solution, following the same procedure described in Ref. [21]. This is implemented by imposing at time  $t_h^0 = 0$  (s) a constant pressure value equal to 2 (atm) throughout the domain, and instantaneous fluctuating

TABLE III. DNS parameters for the auxiliary nonreactive DNS and for the premixed and stratified reactive DNS:  $L$  is the domain length and  $N$  is the number of points used in the  $x$ ,  $y$ , and  $z$  directions, respectively;  $h$  is the channel half-width; NRI: nonreflecting inlet; NRO: nonreflecting outlet; INSW: inert no-slip wall; PERIODIC: cyclic boundary condition.

Case name	$L_x \times L_y \times L_z$	$N_x \times N_y \times N_z$	$\Delta^+$	$x_0/x_L$	$y_0/y_L$	$z_0/z_L$
TCFAUX	$10h \times 2h \times 6h$	$760 \times 360 \times 560$	2.3/1.0/1.9	Periodic	INSW/INSW	Periodic
TCF055h	$10h \times 2h \times 6h$	$2400 \times 480 \times 1440$	0.73	NRI/NRO	INSW/INSW	Periodic
TCF055s	$10h \times 2h \times 6h$	$2400 \times 480 \times 1440$	0.73	NRI/NRO	INSW/INSW	Periodic

velocity, density, and temperature fields computed in the auxiliary nonreacting simulation. This procedure ensures that the flame encounters realistic approaching turbulence from the beginning of the simulation, thereby enabling a relatively short settling time. A one-dimensional premixed laminar flame placed in the middle of the domain is superimposed on the initial velocity field obtained from the auxiliary simulation. Burnt adiabatic product conditions are imposed downstream of the flame and an adjustment of the streamwise component of the velocity field is implemented for compatibility with the lower density on the product side of the flame. A progress variable function  $C$  is used in the initialization to map all points in the three-dimensional domain to one-dimensional CHEMKIN PREMIX [34] solutions for freely propagating planar  $H_2$ -air premixed flames. The progress variable  $C$  is a scalar parametrization of the reactive flow field, based on the water vapour mass fraction, that is equal to zero in the fresh reactants and unity in the burnt products.

The initialization technique described above yields a marginally incorrect initial pressure field. Therefore, an initial ‘‘settling’’ time interval of at least five times the effective acoustic channel transit time [ $10h/c \sim 8.2 \times 10^{-05}$  (s)] is required for the initial pressure fluctuations to exit the domain from the inlet and outlet boundaries. After this initial settling time interval,  $\Delta t_h^{\text{tran}} \sim 4.1 \times 10^{-04}$  (s), the turbulence-flame interaction is no longer affected by the initial pressure fluctuations and at this point the premixed flame has been wrinkled by the approaching turbulence and has begun to propagate upstream.

Following this initial ‘‘start-up’’ transient  $\Delta t_h^{\text{tran}}$ , statistically steady upstream flame propagation occurs in the approaching turbulent channel flow of a lean ( $\phi = 0.55$ ), homogeneous hydrogen-air mixture [22]. After approximately  $1.1 \times 10^{-03}$  (s) of statistically steady upstream flame propagation that has allowed for the acquisition of a satisfactory number of samples for analysis (see below), the inlet boundary condition for the mixture composition is transitioned [beginning at time  $t_s^0 = 1.5 \times 10^{-03}$  (s)] to the stratified mixture distribution with equivalence ratio variation across the channel width as shown in Fig. 2. The total mass flow of the hydrogen fuel entering the channel is slightly increased to emulate the occurrence of a transient surge in the fuel system mass flow that increases the global equivalence ratio of the mixture from  $\phi = 0.55$  to  $\phi \sim 0.7$  temporarily. While remaining overall fuel-lean, the stratified combustion case is designed to be locally fuel-rich at the channel centerline and fuel-lean at the walls. The newly introduced stratified reactants’ mixture is convected downstream with the bulk flow and, as it reaches the turbulent flame brush, at time  $t \sim 2.2 \times 10^{-03}$  approximately, it affects its reactivity, altering the local balance between the flame surface displacement speed and the underlying fluid velocity. A further transition period  $\Delta t_s^{\text{tran}}$  is observed in the solution as the flame adapts to the spatially varying mixture and ultimately results in a drastic change in the global flame shape. The transition from statistically steady premixed to statistically steady stratified flame propagation is completed at time  $t \sim 3.0 \times 10^{-03}$  (s). Sampling of the statistically-steady stratified flame propagation process is initiated at  $t \sim 3.0 \times 10^{-03}$  (s).

Due to the intrinsic transient characteristics of this particular flame configuration, results are sampled relatively frequently at every 1.21 wall time units,  $t_w = 3.3 \times 10^{-05}$  (s). This is to ensure there is a sufficient number of samples in the database for future statistical post-processing. The sampling intervals for the premixed case and for the stratified case are reported in Table IV and result in a total of 27 and 25 samples, respectively. The numerical integration time step is fixed at a

TABLE IV. Overview of settling time intervals and sampling time intervals for the premixed and stratified cases.

Case Name	Time interval name	Description	Actual times
TCF055h	$t_h^0$	PMX DNS starts	$t = 0$ (s)
	$\Delta t_h^{\text{tran}}$	PMX settling time	$0.00 \rightarrow 0.41 \times 10^{-03}$ (s)
	$\Delta t_h$	PMX sampling time	$0.41 \rightarrow 1.50 \times 10^{-03}$ (s)
TCF055s	$t_s^0$	STR DNS starts	$t = 1.50 \times 10^{-03}$ (s)
	$\Delta t_s^{\text{tran}}$	STR settling time	$1.50 \rightarrow 3.00 \times 10^{-03}$ (s)
	$\Delta t_s$	STR sampling time	$3.00 \rightarrow 4.00 \times 10^{-03}$ (s)

value,  $\Delta t = 4.0 \times 10^{-09}$  (s) in the reactive case, and at  $\Delta t = 1.0 \times 10^{-08}$  (s) in the inert auxiliary simulation, corresponding to 8 250 and 3 300 time steps per wall time unit, respectively.

The parallel DNS code, S3D [42], is used to perform the present DNS. In addition to the previous flame-wall interaction study [21,22,30,33], S3D has been used for a range of studies, including a wide range of flame types: premixed flames [43–45], nonpremixed flames [12–15,46,47], stratified [48,49], and autoignition stabilized flames [50–52].

S3D is written in FORTRAN 90 and uses the message passing interface (MPI) for interprocess communication in parallel execution. The algorithm implemented in S3D solves the Navier-Stokes equations for a compressible fluid in conservative form on a structured, Cartesian mesh in one, two, or three spatial directions. Spatial derivatives are computed with an eighth-order, explicit, centered, finite-difference scheme (third-order one-sided stencils are used at the domain boundaries in the nonhomogeneous directions) in conjunction with a tenth-order, explicit, spatial filter, as described in Ref. [53], to remove high-frequency noise and reduce aliasing error. A fourth-order, six-stage, explicit Runge-Kutta scheme, described in Ref. [54], is used for time integration.

The reactive production DNS presented here (premixed and stratified cases including the investigation of hysteresis) were run on 72 000 processor cores (for a total computational cost exceeding 50 M CPUh) on the TITAN architecture that is part the National Center for Computational Science at Oak Ridge NL (ORNL).

### III. RESULTS

In this section DNS of confined turbulent reactive flows are presented, involving flashback in the canonical channel-flow configuration. First, plots of instantaneous and averaged quantities are presented to illustrate the different macroscopic behavior of upstream propagation in the premixed and equivalence ratio-stratified turbulent channel-flow configurations (TCF055h and TCF055s). Then, the local flame structure is illustrated and discussed in detail for the premixed and for the stratified flame. Finally, an analysis of the combustion regimes, as suggested from canonical modeling considerations and observed from the DNS datasets of the two flames, is presented.

#### A. Upstream flame propagation

Turbulent flame propagation, against the channel bulk flow, for the premixed and stratified combustion cases is illustrated and discussed below. The unsteady spatial characteristics of the flashback process lack spatial statistical stationarity and, therefore, the plots presented in Sec. III A 2 are built by spatial averaging of the quantities of interest in the homogeneous spanwise direction at arbitrarily chosen time instants. Comparison of these plots with analogous plots from other times (not shown) confirms the absence of any qualitative and quantitative differences between snapshots of the solution during steady propagation in the time intervals  $\Delta t_h$  and  $\Delta t_s$  for premixed and stratified combustion, respectively.



1. *Instantaneous fields*

Figure 3 illustrates the flame transitioning between premixed and stratified combustion and the drastic effect of the imposed lean-rich-lean fuel distribution across the channel on the global flame shape. Note that the upper wall is not shown and that the surfaces shown in the plots represent:

- (1) The streamwise velocity normalized by the friction velocity,  $u^+ = u/u_\tau$ , on the  $y^+ = 5$  plane (gray-scale contours).
- (2) Hot fluid temperature at  $T = 1700$  (K) (red isosurfaces).
- (3) Back-flow regions characterized by negative streamwise velocity located upstream of the flame surface portions that are convex toward the reactants (blue isosurfaces of  $u^+ = 0$ ).
- (4) The fuel-air equivalence ratio,  $\phi$ , on the  $z^+ = 0$  plane (green-to-white “elevation colourscale” contours).

First, it is clear from the sequence of images in Fig. 3 that the spatial variation in local reactivity across the channel, introduced by stratification of the flammable mixture, causes an abrupt, drastic change in flame shape and propagation topology. The flame reactive surface “flips over,” during the transient  $\Delta t_s^{\text{tran}}$ , and transitions from a propagating mode characterized by the flame front leading-edges located very close to the wall to a radically different propagating mode characterized by a flame front at the channel centerline (V-shaped versus U-shaped propagation). The transition is initiated when the fuel-rich “layer” of the stratified reactants’ mixture, convected downstream by the bulk flow, reaches the two upstream-propagating branches of the V-shaped flame. At that point several relatively large “bumps” form on the reactive flame surface approximately 100 wall units from the walls (at  $y^+ \sim 100$  and  $y^+ \sim 260$ ) and protrude outwards and upstream into the reactants, see Figs. 3(c) and 3(d), ultimately becoming the flame front leading-edge in the bulk of the channel flow, see Figs. 3(e)–3(h).

Second, the change in flame shape induces a subsequent modification of the velocity field in the approaching flow and this has numerous implications on the combustion regime, flame propagation mechanism, and possibly hysteresis effects in the flame-flow interaction. In the premixed combustion case, the fresh reactants’ flow is deflected away from the walls by the two flame fronts that propagate upstream along the walls as relatively thin flame sheets (V-shaped propagation). It is reasonable to assume that most of the fluid expansion caused by these thin reactive sheets happens in the wall-normal direction [22], a process that ultimately leads to the deflection of the near-wall streamlines away from the walls toward the channel centerline and to the acceleration of the bulk flow of the fresh reactants well upstream of the flame; see also Fig. 5(a) below. Furthermore, the mostly flat near-wall branches of the red isosurfaces in Figs. 3(a)–3(d) are evidence of a laminarization of the flow in the hot products that closely approach the solid surface in a spatially uniform pattern. Conversely, in the stratified combustion case, the fresh reactants’ flow is deflected toward the walls by the reactive front leading-edge. This flame front is now propagating upstream in the fuel-rich bulk flow as a wrinkled turbulent flame sheet of relatively flat mean shape (U-shaped propagation). An acceleration of the fresh reactants’ fluid upstream of the flame takes place, in this case, near the walls as clearly evidenced by the gray-to-white transition of  $u^+$  contours at  $y^+ = 5$  in the instantaneous plots of Figs. 3(f)–3(h). This time, as opposed to the premixed case, the fluid acceleration along the walls maintains a relatively high turbulence level in the near-wall regions, as evidenced by the strongly wrinkled red isosurfaces in Figs. 3(e)–3(h), and the hot fluid in the products stream approaches the solid surface in the characteristic pattern dictated by the streaky structures of the boundary layer [30].

An additional important observation that can be made on the basis of the instantaneous plots of Fig. 3 concerns the absence, for the U-shaped propagation mode of the stratified flame, of the reverse flow pockets that have been shown to play a central role in premixed flame flashback [21]. This result highlights the existence of a fundamental difference in the physical mechanism of upstream flame propagation for the two configurations considered here. In the premixed case, the presence of low velocity streaks in the near-wall region of the boundary layer allows the appearance of flow reversals that ultimately enable upstream propagation of the flame front causing flashback while,

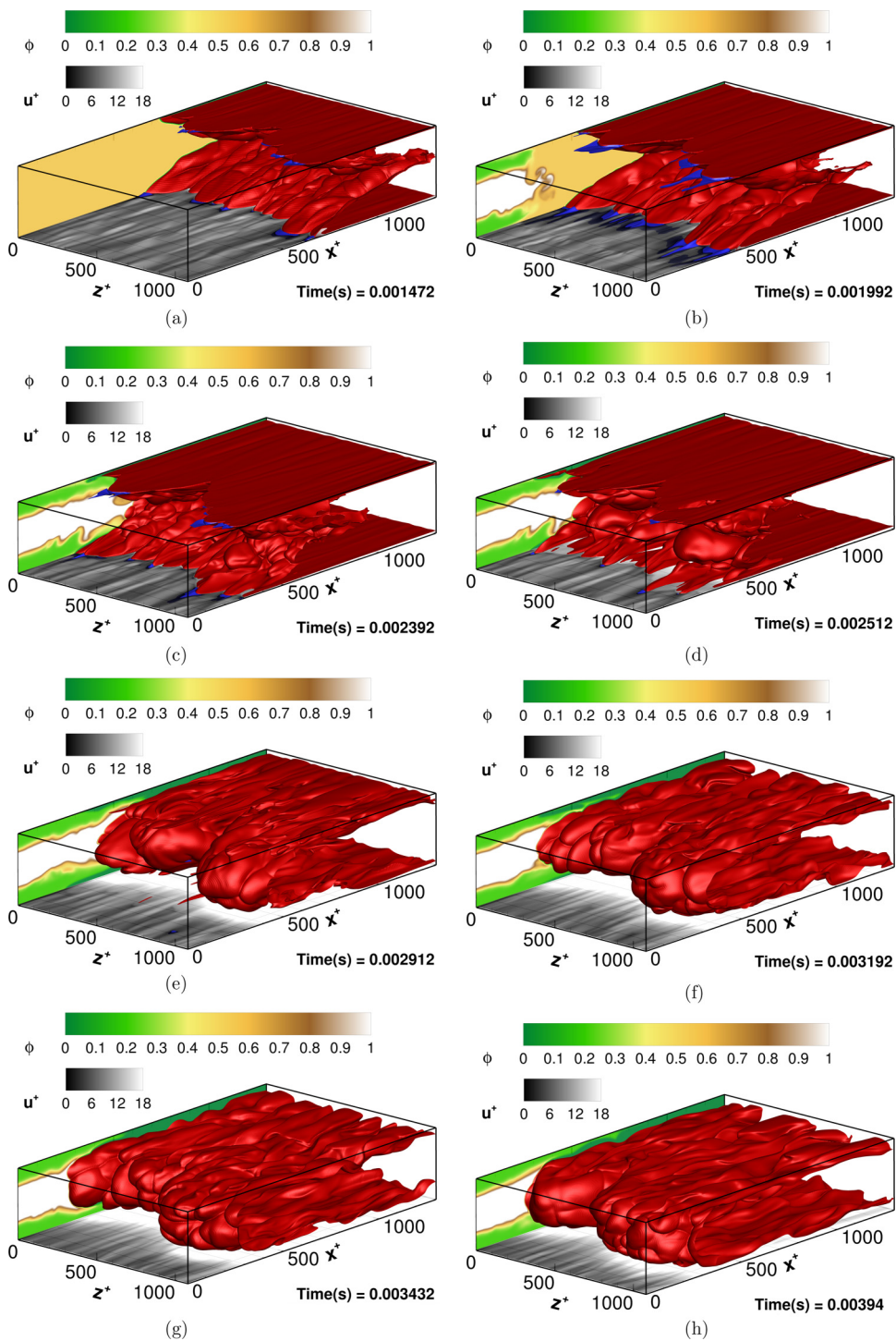


FIG. 3. The transition between premixed combustion and stratified combustion: red isosurfaces demarcate hot fluid temperature at  $T = 1700$  (K), while blue isosurfaces highlight the back-flow regions,  $u^+ = 0$ . The nondimensional streamwise velocity (gray-scale contours) is shown on the  $y^+ = 5$  plane while the equivalence ratio  $\phi$  of the unburnt mixture is illustrated on the  $z^+ = 0$  plane (elevation color-scale contours).

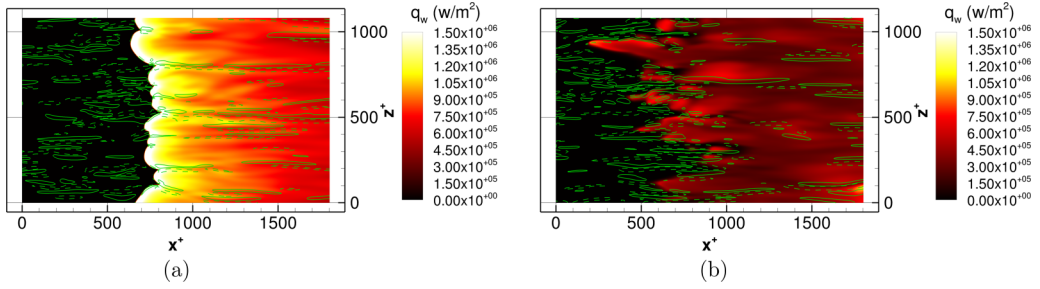


FIG. 4. Instantaneous wall heat flux on the lower wall ( $y^+ = 0$ ) for the premixed (a) and stratified case (b). The streamwise streaky structures of the boundary layer are demarcated by wall-normal vorticity at  $y^+ = 3$  (green lines, solid and dashed lines represent opposite sign of vorticity).

in the stratified case, upstream propagation of the flame front takes place in the bulk flow and its mechanism is therefore unrelated to the streaky structures of the turbulent boundary layer.

Finally, before concluding the present section about the instantaneous fields, it is interesting to mention the considerable difference observed in the wall heat flux instantaneous spatial pattern between the premixed and the stratified case. Figure 4 illustrates the instantaneous wall heat flux on the lower wall during flashback for the premixed flame [Fig. 4(a)] and for the stratified flame [Fig. 4(b)]. While, in the former case, the wall heat flux highest instantaneous values of nearly  $2 \text{ MW/m}^2$  are collocated with the entire length and shape of the flame front, in the latter case the highest values of the heat flux are spatially distributed in a quenching pattern, dictated by the interaction of the flame with the boundary layer streaks, that closely resembles the situation described in Ref. [30]. This observation suggests that the premixed flame quenches directly at the wall along its leading-edge and, due to the low turbulence level in the hot products downstream of the flame, relatively high values of the wall heat flux are present also in the post-flame region.

## 2. Averaged fields

Figure 5 illustrates the spanwise-averaged mean streamwise velocity field, normalized by nominal values of laminar flame speed at  $\phi = 0.55$  and  $\phi = 1.2$ , respectively, and the turbulent fluctuations  $u'_{\text{rms}}$  normalized by the channel bulk flow velocity,  $U_{\text{blk}}$ . The most notable observations from the spatially averaged plots can be summarized as follows:

(1) In the premixed case, the boundary layers in the fresh reactants upstream of the flame surface thickens due to deflection of the streamlines away from the wall and becomes thinner only in the products stream well past the turbulent flame brush.

(2) In the premixed case, the flame front leading edges propagate upstream at a fluid velocity close to zero in the mean (locally in reverse flows).

(3) In the premixed case, the bulk flow “feels” the presence of the flame well upstream of its near-wall leading edges and fluid acceleration is already noticeable more than 300 wall units upstream of the flame fronts. Interestingly, this distance is approximately equal to the flame “depth” defined as the streamwise spatial extent between the flame front leading edges and the the centerline cusp where the two flame branches meet.

(4) In the premixed case, relatively weak velocity fluctuations are present throughout the channel attaining a peak value of  $1/5$  of the bulk flow velocity,  $U_{\text{blk}}$ , at and immediately downstream of the flame front near-wall leading edges.

(5) In the stratified case, the boundary layers in the fresh reactants “feel” the presence of the flame and become thinner due to deflection of the streamlines toward the walls approximately 200 wall units upstream of the flame front.

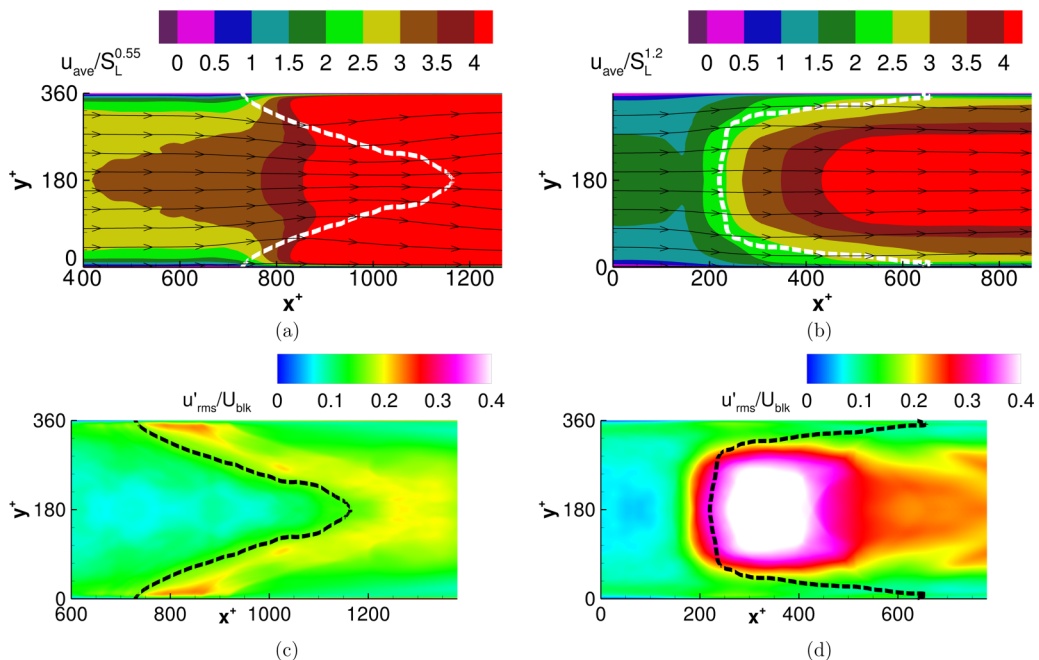


FIG. 5. Mean and fluctuating velocity fields, averaged in the spanwise direction and normalized by the nominal laminar flame speeds (at fuel-rich conditions in the stratified flame case) and by the bulk velocity,  $U_{blk}$ , respectively. The flames are denoted by thick dashed lines corresponding to reaction progress variable,  $C = 0.5$ , and the streamlines by thin black lines with arrowheads for the premixed flame configuration (a)–(c) and for the stratified flame configuration (b)–(d).

381 (6) In the stratified case, the flame front leading edge propagates upstream in the bulk flow  
 382 against an underlying fluid velocity that equals, on average, twice the corresponding laminar flame  
 383 speed of the fuel-rich mixture.

384 (7) In the stratified case, strong velocity fluctuations are present at and immediately downstream  
 385 of the flame front and approximately equal to  $1/3$  to  $1/2$  of the bulk flow velocity,  $U_{blk}$ .

Based in the aforementioned summary, inspection of the averaged fields confirms and quantifies  
 387 many of the qualitative observations of Sec. III A 1. The spatially averaged velocity fields, both  
 388 in the mean and fluctuating parts, inherent to the two flame configurations differ considerably.  
 389 There exist different physical mechanisms that are responsible for the occurrence of flashback in  
 390 the premixed and in the stratified cases. The spatially averaged temperature fields, shown in Fig. 6,  
 391 are consistent with the mean velocity fields presented here and with the considerable differences  
 392 in the instantaneous values of the wall heat fluxes observed in Fig. 4. The thickness of the flame  
 393 brush, in the mean, is visualized by highlighting (in red) its spatial extent between  $C = 0.3$  and  
 394  $C = 0.7$  for premixed and stratified combustion in Figs. 6(c) and 6(c), respectively. The stratified  
 395 case exhibits, in the near-wall regions of the flow, a mean flame brush thickness that is considerably  
 396 larger than that observed in the premixed case (150 versus 50 wall units approximately). An increase  
 397 in the mean flame thickness can be due to two concurrent physical processes. First, the increased  
 398 unsteadiness and wrinkling of the instantaneous stratified flame brush can result in an increase of  
 399 the averaged flame zone thickness. Second, the turbulent length and timescales that characterize  
 400 the motion of the eddies in the approaching turbulence decrease as the distance from the wall is  
 401 reduced, due to deflection and acceleration of the mean flow toward the near-wall regions, while the  
 402 chemical timescales become larger due to locally fuel-lean conditions and heat loss to the wall. The  
 403 simultaneous occurrence of these processes ultimately causes a considerable change in the local  
 404 balance between turbulent and chemical timescales (Damköhler/Karlovitz numbers) that, in turn,

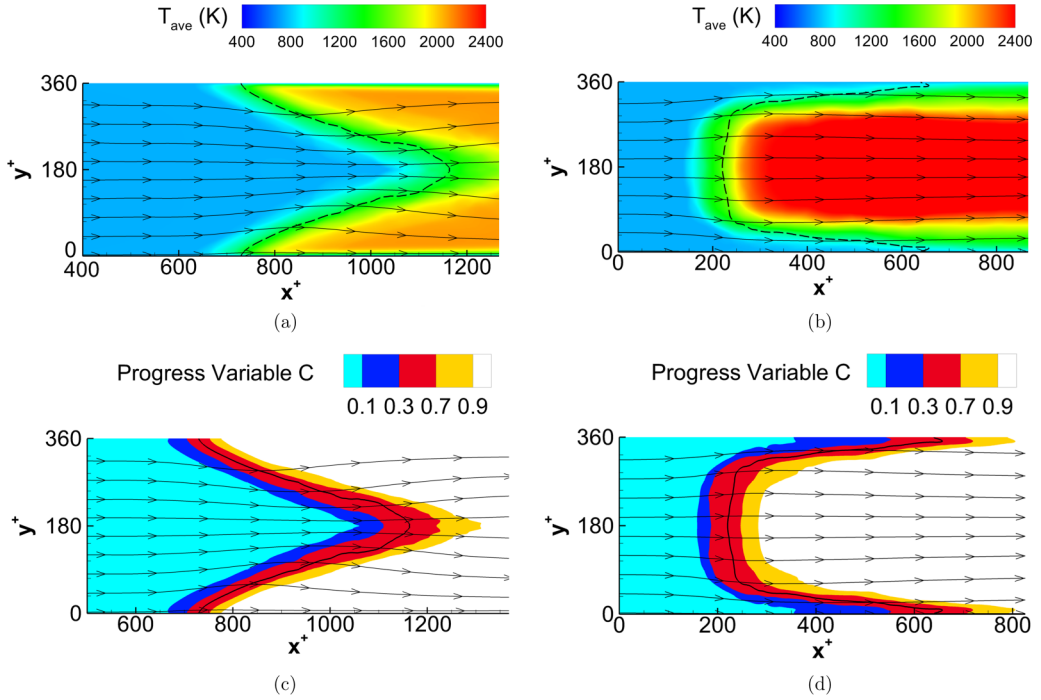


FIG. 6. Mean temperature and reaction progress variable fields, averaged in the spanwise direction, for the premixed flame configuration (a), (c) and for the stratified flame configuration (b), (d). The flame reaction zone is denoted by the black lines corresponding to reaction progress variable,  $C = 0.5$ .

leads to the entrainment of small eddies in the flame reaction zone. This suggests that the flame may undergo a regime change from thin flamelets near the channel centerline to thickened wrinkled flames closer to the wall. This aspect will be discussed more in detail in Ses. III B and III C.

Interestingly, an important common feature characterizes both the premixed and the stratified flame that are, for all other aspects, very different: the slope of the spatially averaged flame surface, represented in Figs. 5 and 6 by the reaction progress variable  $C = 0.5$ , in the immediate vicinity of the walls. Even if the mean flame surface in the stratified case exhibits a shape that is, for the bulk part, convex toward the reactants' side, very close to the wall, for  $y^+ < 10$ , the dashed line demarcating the mean flame surface clearly inverts its slope, corresponding to values of the mean streamwise velocity lower than approximately  $u_{ave}/S_L = 2$ , and approaches the solid, no-slip walls with a slope that is very similar to the one featured in the premixed flame case. This observation suggests the occurrence, within the viscous layer, of similar local balances between flame reactivity, heat loss to the wall and local fluid velocities independent of the actual physical mechanism causing flashback in the channel.

Before concluding the present section about the mean characteristics of the premixed and stratified flames, it is also interesting to consider the eventual occurrence of hysteresis effects in the flow-flame interaction. To this end, the original homogeneous mixture composition is re-introduced at the domain inlet boundary at  $x = 0$  once the end of the sampling time  $\Delta t_s$  [ $t = 4.00e-03$  (s)] for the stratified case is reached. The transient that follows (not shown) reveals the occurrence of a reversal of the sequence illustrated in Figs. 3. Notably, the flame transitions back from the U-shaped to the V-shaped propagation mode. This finding suggests that the flow-flame interaction, for the present configurations, compositional changes and characteristic timescales, is unaffected by hysteresis and that the local reactivity of the reactants mixture approaching the flame is the

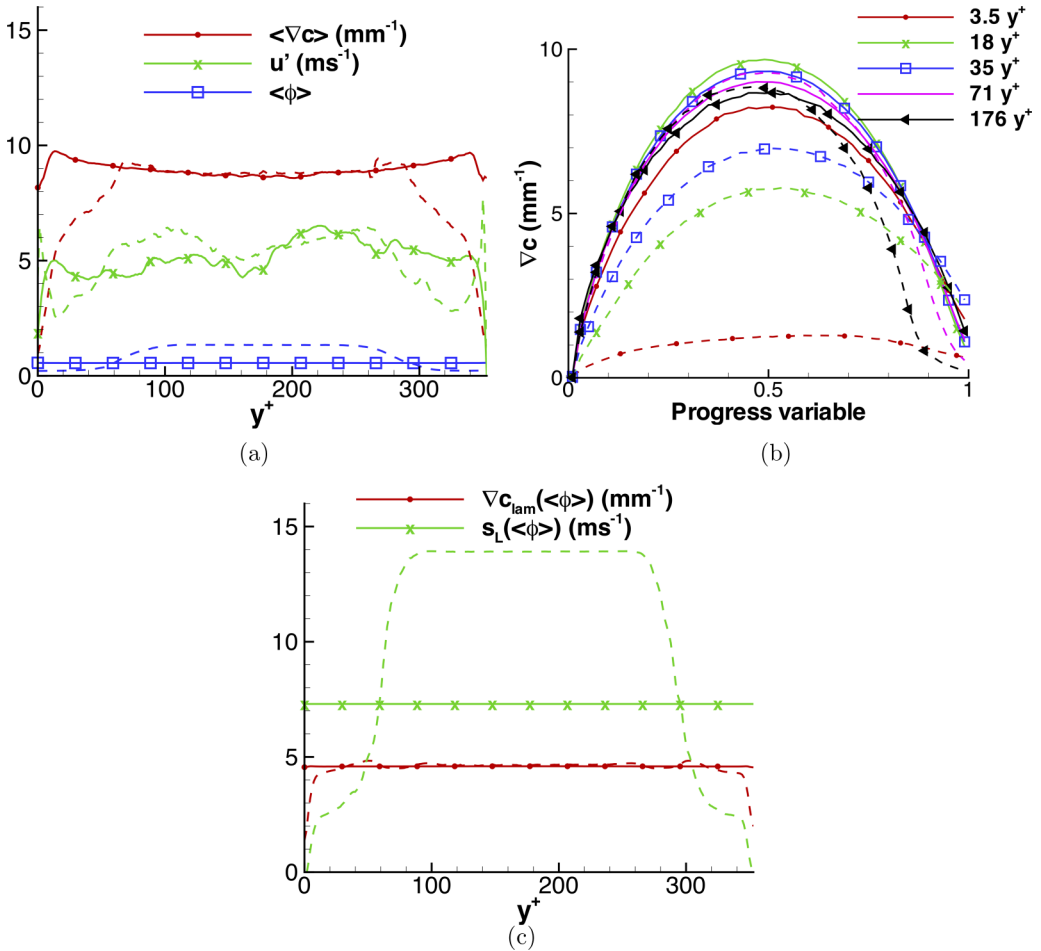


FIG. 7. Variation of the progress variable gradient for the premixed (solid) and equivalence ratio-stratified (dashed) cases: (a) The conditional average progress variable gradient  $\langle \nabla C | C = 0.5 \rangle$ , conditional rms velocity fluctuation  $\langle u'^2 | C = 0.05 \rangle^{1/2}$ , and mean equivalence ratio  $\langle \phi \rangle$  across the channel; (b) the variation of the conditional average progress variable gradient through the flame for several  $y^+$  values; (c) laminar flame values of progress variable gradient  $\nabla C_{\text{lam}}$  and flame speed  $s_L$  as a function of the mean equivalence ratio at the flame location across the channel.

428 main governing parameter controlling the mean flame shape, its propagation mechanism and,  
 429 consequently, the observed flashback characteristics.

430

### B. Local flame structure

431 The local thickness and displacement speed of the flame front are expected to depend on the local  
 432 equivalence ratio, as well as strain and curvature caused by interaction with the turbulent flow. The  
 433 interaction of turbulence and flame structure is assessed by evaluating the local progress variable  
 434 gradient within the flame front. The cross-channel variation of the conditional average progress  
 435 variable gradient,  $\langle \nabla C | C = 0.5 \rangle$ , conditioned on  $C = 0.5$ , is shown in Fig. 7(a) for the premixed  
 436 and equivalence ratio-stratified cases. The figure suggests that the premixed and stratified flames,  
 437 in spite of the considerable differences in mean shape and approach flow field discussed in the  
 438 previous section, are characterized by very similar flame thickness in the bulk flow ( $60 < y^+ <$   
 439  $300$ ). The flame thickness of the equivalence ratio-stratified flame increases ( $\nabla C$  reduces) toward

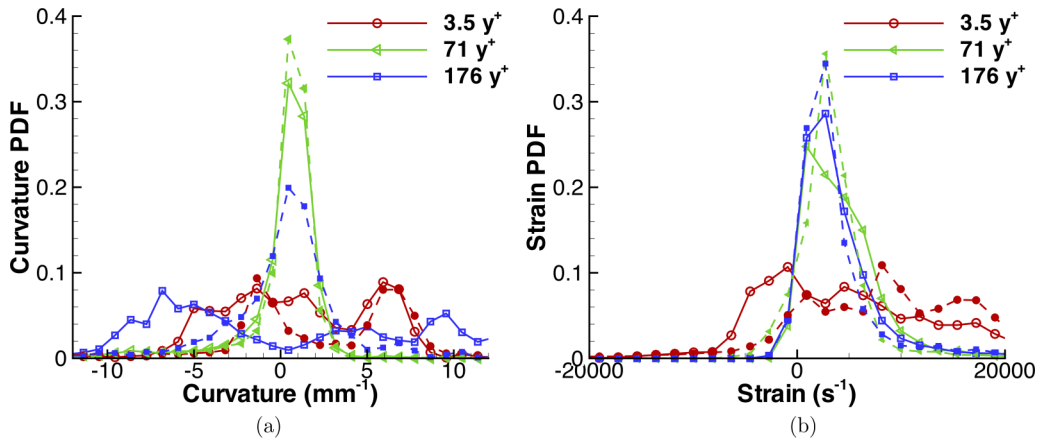


FIG. 8. Probability distributions of (a) curvature and (b) tangential strain rate for the  $C = 0.5$  isosurface at selected wall-normal locations ( $y^+ = 3.5, 71, 176$ ) for the premixed case (solid) and equivalence ratio-stratified case (dashed).

the walls. The variation of progress variable gradient within the flame front is shown by presenting the conditional average  $\langle \nabla C | C \rangle$  versus the progress variable in Fig. 7(b) for the premixed and stratified cases for a range of distances normal to the wall ( $y^+ = 3.5, 18, 35, 71, 176$ ). The thickness of the premixed flame reduces slightly at  $y^+ = 3.5$ , possibly due to effects of wall heat transfer and reduced tangential strain, however the shape of the gradient profile is similar at all wall-normal positions in the premixed flame. For the stratified flame, the shape of the progress variable gradient profile varies significantly from the center of the channel toward the wall, with progressive flattening of the low-progress variable preheat region approaching the wall. The migration of the peak gradient from lower to higher progress variables is partly associated with the variation of equivalence ratio, but thickening of the preheat layer may also be indicative of a change in combustion regime.

A representative value for the turbulent velocity fluctuations  $u'$  ahead of the flames is obtained by evaluating the conditional root mean square velocity fluctuation  $\langle u'^2 | C = 0.05 \rangle^{1/2}$  within the preheat layer at  $C = 0.05$ . The  $u'$  profiles differ between the premixed and stratified flames; in particular, the stratified case displays a peak in turbulent fluctuations at  $y^+ < 5$  (see Sec. III C for more details on this specific topic). However, the increase in flame thickness of the stratified flame near the walls is more closely associated with the variation of equivalence ratio shown in Fig. 7(a). The effect of the equivalence ratio variation on flame behavior is illustrated in Fig. 7(c) by presenting the mean variation of equivalence ratio across the channel and its effect on the progress variable gradient (at  $C = 0.5$ ) and the propagation speed of freely-propagating planar laminar premixed flames. The laminar flame thickness of hydrogen-air flames determined from H<sub>2</sub>O-based progress variable gradients is relatively insensitive to the wide variation of equivalence ratio that characterize the stratified channel flow until the equivalence ratio decreases below 0.25 very close to the walls. In contrast, the equivalence ratio has a marked influence on the laminar flame speed in the region where the local flame thickness is seen to increase in the equivalence ratio-stratified turbulent flame. Therefore, the variation of flame thickness in the equivalence ratio-stratified case is largely controlled by an increasing influence of turbulence within the flame, associated with the variation of  $u'/s_L$ , rather than by the direct effect of equivalence ratio on local flame front thickness.

The probability density function (PDF) of local flame curvature and tangential strain rate are shown in Figs. 8(a) and 8(b) for a flame surface defined by  $C = 0.5$ . Positive curvature corresponds to “bulges” convex toward the reactants and negative curvature corresponds to “cusps” concave toward the reactants. The curvature distribution in the premixed flame shows a prevalence of large negative curvature around the centerline  $y^+ \sim 176$ , corresponding to cusps at the apex of the V-shaped flame. In contrast, the curvature distribution in the stratified flame is approximately

473 symmetric in the center of the channel. The curvature distribution in the stratified flame has a large  
 474 positive mean at  $y^+ = 3.5$ , indicating the prevalence of convex flame bulges as the flame decelerates  
 475 toward the wall. At intermediate positions,  $y^+ = 71$ , both the premixed and stratified flames are  
 476 characterised by mean curvature close to zero with a negatively skewed distribution, corresponding  
 477 to bulges of flame meeting at sharp cusps.

478 Figure 8(b) indicates that both flames are characterised by positive mean (extensive) tangential  
 479 strain and by positive skewness toward rare highly extensive strain events. The most significant  
 480 difference between the premixed and equivalence ratio-stratified flames appears close to the wall (at  
 481  $y^+ = 3.5$ ) where the premixed flame exhibits a significant contribution from negative (compressive)  
 482 tangential strain, characteristic of dilation-driven flame alignment, while tangential strain in the  
 483 stratified flame remains almost entirely extensive. This may be attributed to the vastly lower  
 484 contribution of dilatation in the extremely lean mixture at the wall in the stratified case.

### 485 C. Combustion regimes

486 An accurate prediction of the combustion regimes that characterize flashback in channels and  
 487 ducts is of primary importance for CFD modeling (RANS, LES) in engineering applications. Most  
 488 turbulent combustion models routinely utilized in RANS and LES computations are highly tuned  
 489 to specific combustion regimes, i.e., multiregime models are complex and not widely adopted yet  
 490 as they require metrics that delineate the spatiotemporal boundaries between different modes of  
 491 combustion. Combustion regimes can be described quantitatively by the nondimensional Damköhler  
 492 and Karlovitz numbers, both representing the ratio between chemical and turbulent time or length  
 493 scales that characterize the specific reactive flow, and where energy-containing and dissipative  
 494 turbulent scales are used, respectively [55].

495 In turbulent channel flows the viscous (wall) time and length scales,  $t_w$  and  $\delta_v$ , represent well-  
 496 defined quantities that uniquely characterize the flow. Therefore, in Ref. [30] we proposed to utilize  
 497 the wall timescale  $t_w$ , and specifically its value in the undisturbed fresh reactants' flow, to provide  
 498 a simple, unique ratio to the nominal flame timescale  $t_l$ : the wall-based Damköhler number  $Da^w =$   
 499  $t_w/t_l$ , see Table II in Sec. II that characterizes the combustion regime in turbulent reactive channel  
 500 flows. However, in situations where the turbulent and chemical scales span a wide range of values  
 501 within the same flow, the single valued estimate provided by  $Da^w$  may not, in general, be able  
 502 to accurately delineate variations in combustion regimes. The present DNS datasets correspond to  
 503 reactive flow configurations that exhibit spatial variations in the turbulent and chemical timescales  
 504 simultaneously (due to stratification and heat loss) and, hence, can be used to assess the accuracy  
 505 of  $Da^w$  to predict the combustion regime(s) occurring across the entire channel width. Furthermore,  
 506 for those configurations in which  $Da^w$  is inaccurate in delineating the different regimes, we propose  
 507 to construct a *nominal* channel-flow Karlovitz number  $Ka_{in}^{ch}$  that provides improved local estimates  
 508 of the combustion regime as a function of the wall distance.  $Ka_{in}^{ch}$  is constructed by utilizing wall-  
 509 normal profiles of the *nominal* dissipative timescale  $t_\eta = (\nu/\epsilon)^{1/2}$  from nonreacting, fully developed  
 510 channel flows and of the *nominal* chemical timescale  $t_l = \delta_l/S_l$  from a table of unstretched laminar  
 511 premixed flames with consistent stoichiometry; see Fig. 9(a) with the actual mixture conditions from  
 512 the stratified case.  $Ka_{in}^{ch}$  is therefore a *nominal* quantity that can be constructed from tabulated data  
 513 from turbulent nonreactive channel flows and premixed laminar flames.

514 Figures 9(b) and 9(c) illustrate a comparison of the *nominal* channel-flow Karlovitz number,  
 515  $Ka_{in}^{ch}$  (green lines), against the *effective* Karlovitz number,  $Ka_{fl}^{ch}$ , observed in the immediate vicinity  
 516 of the flame reaction zone (black symbols), where the latter is constructed by sampling local values  
 517 of  $t_\eta$  and  $t_l$  conditional on the reaction progress variable,  $C$ , between the 0.1 and 0.3 bounds, i.e.,  
 518 these enclose the blue coloured region in Figs. 6(c) and 6(d). In the premixed flame case there is  
 519 relatively good agreement between the effective channel-flow Karlovitz number and the nominal  
 520 one which slightly underpredicts the ratio of chemical to turbulent timescales observed at the flame  
 521 surface. Both combustion regime estimates, the nominal and the effective one, are less than  $Ka = 1$ ,  
 522 spanning a range of values between 0.4 and 0.9 across the channel. This suggests that the premixed



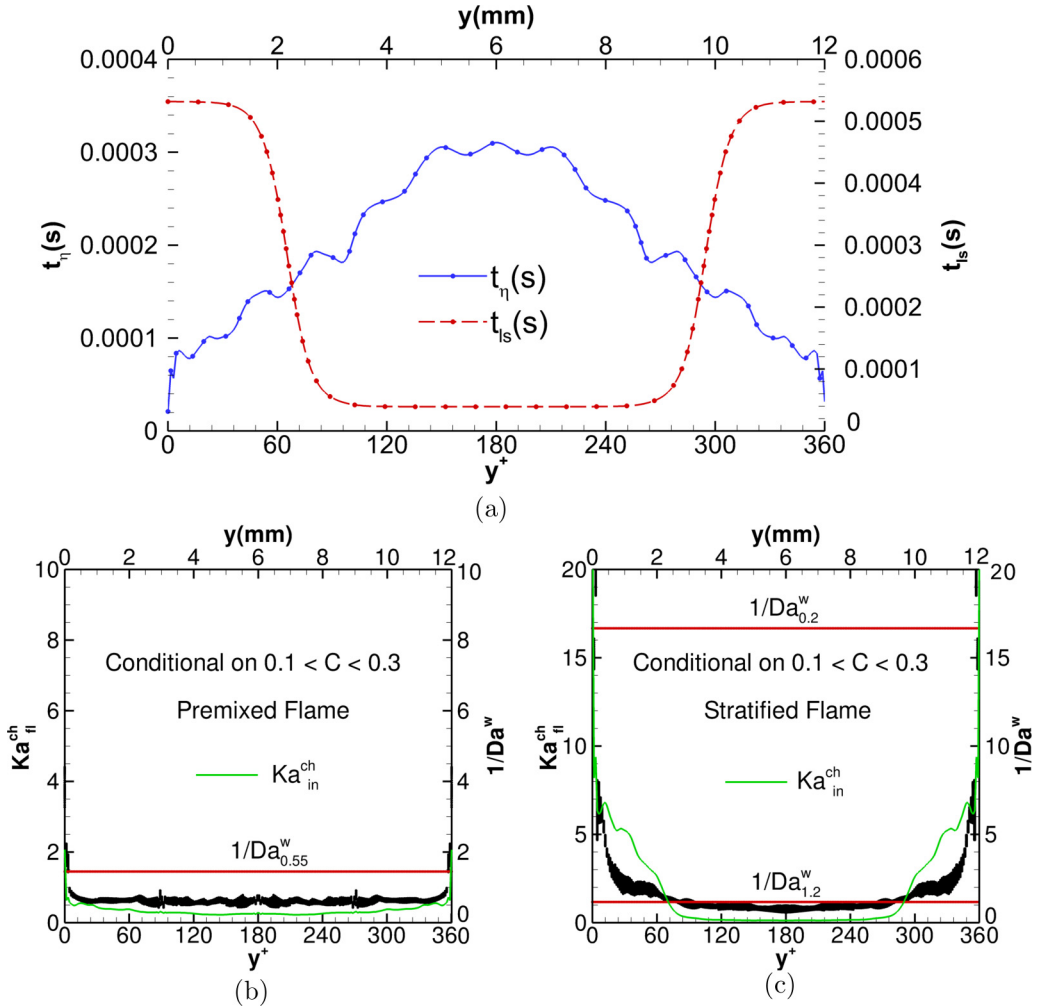


FIG. 9. Wall-normal profiles of turbulent and chemical timescales,  $t_\eta$  (blue line and symbols) and  $t_{is}$  (red line and symbols), are shown at the channel inlet for the stratified combustion case (a). Wall-normal profiles of the *nominal* channel-flow Karlovitz number at the channel inlet plane  $Ka_{in}^{ch}$  (green line) and of the *effective* Karlovitz number sampled immediately upstream of the flame  $Ka_{in}^{ch}$  (black symbols, conditionally sampled on  $0.1 < C < 0.3$ ) are shown in the premixed (b) and stratified flame case (c). The reciprocal of the relevant wall Damköhler numbers,  $Da^w$ , is also shown (horizontal red lines).

flame is in the “thin flamelets” combustion regime. Note that the single-valued estimate from the wall Damköhler number  $Da^w$  is relatively similar to the other two although slightly above unity ( $1/Da^w = 1/0.69 = 1.45$ ). In the stratified flame case  $Ka_{in}^{ch}$  underpredicts  $Ka_{in}^{ch}$  in the bulk flow and overpredicts it in the intermediate regions while agreement is quite good near the wall. Clearly both the nominal and the effective Karlovitz number suggest the coexistence of two combustion regimes in the stratified flame configuration: “thin flamelets” in the bulk flow for  $Ka < 1$  and “thickened flamelets” in the near-wall regions for  $1 < Ka < 10$ . It is interesting to note that the present observation of a transition from “thin flamelets” in the bulk flow to “thickened flamelets” near the walls is in good accordance with earlier results from the anchored V-flame configuration [30], characterized by similar mean flame shape (flame leading edge at the channel centerline), and with more recent findings from a DNS study of a turbulent head-on quenching configuration

523  
524  
525  
526  
527  
528  
529  
530  
531  
532  
533

534 [56], characterized by similar mean direction of the flame-wall interaction (flame brush quenches  
535 perpendicularly to the wall).

#### 536 **D. Implications for flashback modeling**

537 The validation of turbulent combustion models is clearly beyond the scope of the present  
538 paper; nevertheless, the observations reported in the above sections provide important guidelines  
539 for the choice, development, and assessment of such models' ability to represent flame flashback  
540 and we summarize these here. This is especially important, and can be of great value, for more  
541 applied modeling in connection with RANS and LES approaches that are characterized by lower  
542 computational requirements. First, the results presented in Sec. III A clearly establish that, while  
543 accurate prediction of the premixed flame near-wall propagation requires DNS-like resolution of  
544 the characteristic structures of the wall boundary layer, the stratified flame propagation in the bulk  
545 flow is governed by the local turbulent flame velocity and modulated by a relatively homogeneous  
546 and more isotropic turbulence present near the channel centerline. Second, the discussion from  
547 Sec. III C provides a promising methodology that can be used to estimate the combustion regime of  
548 the stratified flame's leading edge that effectively controls propagation of that flame type to the first  
549 order. Accordingly, for the present case of relatively low Karlovitz numbers, turbulent combustion  
550 models based on the assumption of a well-defined flame structure (e.g., flamelet, thickened flame,  
551 and flame surface density approaches) seem well-equipped to predict the stratified flame flashback  
552 accurately because they provide an accurate description of the main governing process: turbulent  
553 flame propagation in the bulk flow. As for the premixed flame flashback, general-purpose turbulent  
554 combustion models such as those mentioned above are not well-suited to accurately capture the main  
555 aspects of this process because it is controlled by details of the near-wall dynamics of the turbulent  
556 boundary layer that are unresolved in RANS or wall-modeled LES. As promising alternatives,  
557 less general and more empirical approaches [22,24] have shown encouraging results but their  
558 applicability is, of course, uncertain outside of the envelope of the datasets used to build them.

## 559 **IV. CONCLUSIONS**

560 We performed three-dimensional DNSs of upstream flame propagation in fully-developed  
561 turbulent plane channel flow for premixed and stratified hydrogen/air flames. The present study  
562 complements earlier work [21,22] and reports a comparison of the flames' shape, structure, and  
563 propagation mechanism in a fuel-lean homogeneous mixture characterized by an equivalence  
564 ratio of  $\phi = 0.55$  (premixed flame) and in a globally fuel-lean, nonhomogeneous mixture whose  
565 equivalence ratio varies between  $\phi = 0.2$  at the walls and  $\phi = 1.2$  in the bulk flow (stratified  
566 flame). The pressure and temperature of the H<sub>2</sub>/air mixtures is kept the same as in earlier cases,  
567 at  $P = 2$  (atm) and  $T_u = 750$  (K), respectively. The aim of the present DNS study is to investigate  
568 the effect of fuel-oxidant mixture stratification on the mechanism of flame flashback in turbulent  
569 boundary layers and its implications for the co-existence of multiple combustion regimes.

570 The introduction of a compositional inhomogeneous reactants' mixture with a fuel lean-rich-lean  
571 profile across the channel leads to an abrupt change in the physical mechanism of flame propagation  
572 and, in turn, ultimately results in an abrupt change in flame shape and associated flow pattern. In the  
573 premixed configuration (homogeneous mixture) the leading edges of the flame front propagate in  
574 the near-wall regions of the turbulent boundary layer, exploiting the low-velocity, streaky coherent  
575 structures as they creep upstream under the bulk flow. Conversely, in the stratified configuration  
576 (nonhomogeneous mixture) the leading edges of the flame front propagate in the bulk flow due to  
577 the high reactivity of the fuel-rich mixture injected near the channel centerline. While in the former  
578 case the approach flow is deflected away from the walls by the near-wall flame front, in the latter  
579 the opposite occurs and the flow is deflected and accelerated toward the walls where turbulence  
580 production occurs. As a consequence, the near-wall fuel-lean flame brush encounters relatively  
581 strong turbulence ultimately resulting in a combustion regime transition from thin flamelets  $Ka < 1$

to thickened flamelets  $Ka \sim 10$ . Conditionally sampled data (for  $C = 0.5$ ) confirms local thickening of the stratified flame in the near-wall fuel-lean regions of the channel exhibiting lower values of  $\nabla C$  (versus  $y^+$  and  $C$  itself) and the dominance of positive (extensive) strain of the flame surface with the notable exception, in the premixed flame case, of the locations where reverse flow occurs.

Furthermore, we provide a method to estimate the cross-channel variation of a *nominal* Karlovitz number constructed using canonical timescales for the turbulence and chemistry. Comparison against an *effective* Karlovitz number, computed locally from the DNS data just upstream of the flame reaction layer, reveals a satisfactory agreement between the two. In spite of some level of disagreement observed locally, the present results seem to suggest that the nominal channel-flow Karlovitz,  $Ka_{in}^{ch}$ , provides an accurate envelope to its effective counterpart,  $Ka_{fl}^{ch}$ . Hence, this implies that an estimate based on  $Ka_{in}^{ch}$  can be used to provide an assessment of the combustion regime(s) that characterizes wall-bounded reactive flows in general and can therefore help modelers in selecting the appropriate turbulent combustion modeling approach.

Finally, it is important to recognize that the present analysis has been performed on DNS datasets built at relatively low Reynolds numbers, as it is often the case due to computational cost, and this fact puts some limitations on a broader interpretation of the results. Typically, flashback in gas turbine burners happens at high pressure and high Reynolds number conditions. The current DNS study therefore leaves open a number of important research questions, including: What is the Reynolds number scaling on the near-wall structures of the turbulent boundary layer that facilitate flashback of the premixed flame along the channel walls? Is the mechanism of upstream flame propagation qualitatively unchanged at higher Reynolds number for the premixed and stratified flames? Given the present limitations of the DNS approach, even in a supercomputing context, laboratory experiments could answer some of these questions. A potentially interesting avenue of investigation that should be pursued experimentally is related to the role on flame flashback of the very large “super structures” that, while recently observed in channel flows at high Reynolds numbers ( $Re_\tau > 1000$ ) using advanced visualization and post-processing techniques [57], are still beyond the reach of combustion DNS. The presence within the turbulent channel flow of a spatially asymmetric and temporally unsteady meandering “quiescent” core, characterized by high mean longitudinal velocities and low velocity fluctuations level, is likely to have important effects on the mechanisms of upstream flame propagation and result in disruption of the symmetric flame shapes observed here during steady propagation. Intermittently introducing large spatial asymmetries in the channel-flow velocity field (see Fig. 11 in Ref. [57]), these large-scale “super structures” can potentially enhance or hinder flame flashback depending on the relative size of their timescale compared to the flame’s own response timescale and to its ability to adapt to changes in the approaching flow field.

## ACKNOWLEDGMENTS

The work at SINTEF has been supported by the BIGCCS Centre, performed under the Norwegian research program Centres for Environmental-friendly Energy Research (FME). The work at the University of Southampton has been supported by EPSRC Grant No. EP/L002698/1. The work at Sandia National Laboratories was supported by the U.S. Department of Energy, Office of Basic Energy Sciences, Division of Chemical Sciences, Geosciences, and Biosciences. Sandia National Laboratories is a multimission laboratory managed and operated by National Technology and Engineering Solutions of Sandia, LLC., a wholly owned subsidiary of Honeywell International, Inc., for the U.S. Department of Energy’s National Nuclear Security Administration under Contract No. DE-NA-0003525. The views expressed in the article do not necessarily represent the views of the U.S. Department of Energy or the United States Government. The computational allocation for the present study was provided by the National Infrastructure for High Performance Computing and Data Storage in Norway (Project No. nn9121k) and by the National Center for Computational Sciences at Oak Ridge National Laboratory, which is supported by the Office of Science of the U.S. Department of Energy under Contract No. DE-AC05-00OR22725.

- [1] F. Biagioli, Stabilization mechanism of turbulent premixed flames in strongly swirled flows, *Combust. Theory Model.* **10**, 389 (2006).
- [2] J. Fritz, M. Kröner, and T. Sattelmayer, Flashback in a swirl burner with cylindrical premixing zone, *ASME: J. Eng. Gas Turbines Power* **126**, 276 (2004).
- [3] A. Kalantari and V. McDonell, Boundary layer flashback of nonswirling premixed flames: Mechanisms, fundamental research, and recent advances, *Prog. Energy Combust. Sci.* **61**, 249 (2017).
- [4] M. Brower, E. L. Petersen, W. K. Metcalfe, H. J. Curran, M. Füre, G. Bourque, N. Aluri, and F. Güthe, Ignition delay time and laminar flame speed calculations for natural gas/hydrogen blends at elevated pressures, *ASME: J. Eng. Gas Turbines Power* **135**, 021504 (2013).
- [5] N. Donohoe, A. Heufer, W. K. Metcalfe, H. J. Curran, M. L. Davis, O. Mathieu, D. Plichta, A. Morones, E. L. Petersen, and F. Güthe, Ignition delay times, laminar flame speeds, and mechanism validation for natural gas/hydrogen blends at elevated pressures, *Combust. Flame* **161**, 1432 (2014).
- [6] A. Sanchez and F. A. Williams, Recent advances in understanding of flammability characteristics of hydrogen, *Prog. Energy Combust. Sci.* **41**, 1 (2014).
- [7] F. Dabireau, B. Cuenot, O. Vermorel, and T. Poinsot, Interaction of flames of  $H_2 + O_2$  with inert walls, *Combust. Flame* **135**, 123 (2003).
- [8] P. Chiesa, G. Lozza, and L. Mazzocchi, Using hydrogen as gas turbine fuel, *ASME: J. Eng. Gas Turbines Power* **127**, 73 (2005).
- [9] D. Ebi and N. Clemens, Experimental investigation of upstream flame propagation during boundary layer flashback of swirl flames, *Combust. Flame* **168**, 39 (2016).
- [10] D. Ebi, R. Ranjan, and N. Clemens, Coupling between premixed flame propagation and swirl flow during boundary layer flashback, *Exp. Fluids* **59**, 109 (2018).
- [11] A. R. Masri, Partial premixing and stratification in turbulent flames, *Proc. Combust. Inst.* **35**, 1115 (2015).
- [12] R. W. Grout, A. Gruber, C. S. Yoo, and J. H. Chen, Direct numerical simulation of flame stabilization downstream of a transverse fuel jet in cross-flow, *Proc. Combust. Inst.* **33**, 1629 (2011).
- [13] R. W. Grout, A. Gruber, H. Kolla, P.-T. Bremer, J. C. Bennet, A. Gyulassy, and J. H. Chen, A direct numerical simulation study of turbulence and flame structure in transverse jets analysed in jet-trajectory based coordinates, *J. Fluid Mech.* **706**, 351 (2012).
- [14] H. Kolla, R. W. Grout, A. Gruber, and J. H. Chen, Mechanisms of flame stabilization and blowout in a reacting turbulent hydrogen jet in cross-flow, *Combust. Flame* **159**, 2755 (2012).
- [15] Y. Minamoto, H. Kolla, R. W. Grout, A. Gruber, and J. H. Chen, Effect of fuel composition and differential diffusion on flame stabilization in reacting syngas jets in turbulent cross-flow, *Combust. Flame* **162**, 3569 (2015).
- [16] F. Biagioli and F. Güthe, Effect of pressure and fuel-air unmixedness on  $NO_x$  emissions from industrial gas turbine burners, *Combust. Flame* **151**, 274 (2007).
- [17] B. Lewis and G. von Elbe, Stability and structure of burner flames, *J. Chem. Phys.* **11**, 75 (1943).
- [18] A. Dreizler and B. Böhm, Advanced laser diagnostics for an improved understanding of premixed flame-wall interactions, *Proc. Combust. Inst.* **35**, 37 (2015).
- [19] C. Eichler and T. Sattelmayer, Premixed flame flashback in wall boundary layers studied by long-distance micro-PIV, *Exp. Fluids* **52**, 347 (2012).
- [20] C. Heeger, R. L. Gordon, M. J. Tummers, T. Sattelmayer, and A. Dreizler, Experimental analysis of flashback in lean premixed swirling flames: Upstream flame propagation, *Exp. Fluids* **49**, 853 (2010).
- [21] A. Gruber, J. H. Chen, D. Valiev, and C. K. Law, Direct numerical simulation of premixed flame boundary layer flashback in turbulent channel flow, *J. Fluid Mech.* **709**, 516 (2012).
- [22] A. Gruber, A. R. Kerstein, D. Valiev, C. K. Law, H. Kolla, and J. H. Chen, Modelling of mean flame shape during premixed flame flashback in turbulent boundary layers, *Proc. Combust. Inst.* **35**, 1485 (2015).
- [23] G. Baumgartner, Lorenz R. Boeck, and T. Sattelmayer, Experimental investigation of the transition mechanism from stable flame to flashback in a generic premixed combustion system with high-speed micro-PIV and micro-PLIF combined with chemiluminescence imaging, in *Proceedings of the ASME Turbo Expo 2015, June 15–19, 2015, Montreal, Canada* (American Society of Mechanical Engineers, New York, 2015), pp. GT2015–42605.

- [24] V. Hoferichter, C. Hirsch, and T. Sattelmayer, Analytic prediction of unconfined boundary layer flashback limits in premixed hydrogen-air flames, *Combust. Theory Model.* **21**, 382 (2017).
- [25] B. Fine, The flashback of laminar and turbulent burner flames at reduced pressure, *Combust. Flame* **2**, 253 (1958).
- [26] L. Khitritin, P. Moin, D. Smirnov, and V. Shevchuk, Peculiarities of laminar- and turbulent-flame flashbacks, *Symp. (Int.) Combust.* **10**, 1285 (1965).
- [27] V. N. Kurdyumov, E. Fernandez, and A. Linan, Flame flashback and propagation of premixed flames near a wall, *Proc. Combust. Inst.* **28**, 1883 (2000).
- [28] V. N. Kurdyumov and E. Fernandez-Tarrazo, Lewis number effect on the propagation of premixed laminar flames in narrow open ducts, *Combust. Flame* **128**, 382 (2002).
- [29] V. N. Kurdyumov, E. Fernandez-Tarrazo, J. M. Truffaut, J. Quinard, A. Wangher, and G. Searby, Experimental and numerical study of premixed flame flashback, *Proc. Combust. Inst.* **31**, 1275 (2007).
- [30] A. Gruber, R. Sankaran, E. R. Hawkes, and J. H. Chen, Turbulent flame-wall interaction: A direct numerical simulation study, *J. Fluid Mech.* **658**, 5 (2010).
- [31] C. Eichler and T. Sattelmayer, Experiments on flame flashback in a quasi-2D turbulent wall boundary layer for premixed methane-hydrogen-air mixtures, *ASME: J. Eng. Gas Turbines Power* **133**, 011503 (2011).
- [32] C. Eichler, G. Baumgartner, and T. Sattelmayer, Experimental investigation of turbulent boundary layer flashback limits for premixed hydrogen-air flames confined in ducts, in *Proceedings of ASME Turbo Expo 2011, June 6–10, 2011, Vancouver, Canada* (American Society of Mechanical Engineers, New York, 2011), pp. GT2011–45362.
- [33] A. Gruber, P. S. Salimath, and J. H. Chen, Direct numerical simulation of laminar flame-wall interaction for a novel H<sub>2</sub>-selective membrane/injector configuration, *Int. J. Hydrogen Energy* **39**, 5906 (2014).
- [34] R. J. Kee, G. Dixon-Lewis, J. Warnatz, M. E. Coltrin, J. A. Miller, and H. K. Moffat, *A Fortran Chemical Kinetics Package for the Analysis of Gas-Phase Chemical Kinetics*, Tech. Rep. Release 3.5 (Reaction Design Inc., San Diego, CA, 1999).
- [35] J. Li, Z. Zhao, A. Kazarov, and F. L. Dryer, An updated comprehensive kinetic model of hydrogen combustion, *Int. J. Chem. Kinet.* **36**, 566 (2004).
- [36] T. Poinso and S. K. Lele, Boundary conditions for direct simulations of compressible viscous flow, *J. Comput. Phys.* **101**, 104 (1992).
- [37] J. C. Sutherland and C. A. Kennedy, Improved boundary conditions for viscous, reactive, compressible flows, *J. Comput. Phys.* **191**, 502 (2003).
- [38] C. S. Yoo, Y. Wang, A. Trouvé, and H. G. Im, Characteristic boundary conditions for direct simulations of turbulent counterflow flames, *Combust. Theory Model.* **9**, 617 (2005).
- [39] C. S. Yoo and H. G. Im, Characteristic boundary conditions for simulations of compressible reacting flows with multi-dimensional, viscous and reaction effects, *Combust. Theory Model.* **11**, 259 (2007).
- [40] A. Gruber, Direct numerical simulation of turbulent combustion near solid surfaces, Doctoral thesis, Norwegian University of Science and Technology, 2006.
- [41] R. Moser, J. Kim, and N. Mansour, Direct numerical simulation of turbulent channel flow up to  $Re_\tau = 590$ , *Phys. Fluids* **11**, 943 (1999).
- [42] J. H. Chen, A. Choudhary, B. de Supinski, M. DeVries, E. R. Hawkes, S. Klasky, W. K. Liao, K. L. Ma, J. Mellor-Crummey, N. Podhorski, R. Sankaran, S. Shende, and C. S. Yoo, Terascale direct numerical simulations of turbulent combustion using S3D, *Comput. Sci. Discov.* **2**, 015001 (2009).
- [43] E. R. Hawkes and J. H. Chen, Evaluation of models for flame stretch due to curvature in the thin reaction zones regime, *Proc. Combust. Inst.* **30**, 647 (2005).
- [44] R. Sankaran, E. R. Hawkes, J. H. Chen, T. Lu, and C. K. Law, Structure of a spatially developing turbulent lean methane-air Bunsen flame, *Proc. Combust. Inst.* **31**, 1291 (2007).
- [45] E. R. Hawkes, O. Chatakonda, H. Kolla, A. R. Kerstein, and J. H. Chen, A petascale direct numerical simulation study of the modeling of flame wrinkling for large-eddy simulations in intense turbulence, *Combust. Flame* **159**, 2690–2703 (2012).

- [46] E. R. Hawkes, R. Sankaran, J. C. Sutherland, and J. H. Chen, Scalar mixing in direct numerical simulations of temporally evolving plane jet flames with skeletal CO/H<sub>2</sub> kinetics, *Proc. Combust. Inst.* **31**, 1633 (2007).
- [47] C. S. Yoo, R. Sankaran, and J. H. Chen, Three-dimensional direct numerical simulation of a turbulent lifted hydrogen jet flame in heated coflow: Flame stabilization and structure, *J. Fluid Mech.* **640**, 453 (2009).
- [48] E. S. Richardson and J. H. Chen, Analysis of turbulent flame propagation in equivalence ratio-stratified flow, *Proc. Combust. Inst.* **36**, 1729 (2017).
- [49] H. Wang, E. R. Hawkes, B. Savard, and J. H. Chen, Direct numerical simulation of a high Ka CH<sub>4</sub>/air stratified premixed jet flame, *Combust. Flame* **193**, 229 (2018).
- [50] T. Echehki and J. H. Chen, Direct numerical simulation of autoignition in nonhomogeneous hydrogen-air mixtures, *Combust. Flame* **134**, 169 (2003).
- [51] R. Sankaran, H. G. Im, E. R. Hawkes, and J. H. Chen, The effects of non-uniform temperature distribution on the ignition of a lean homogeneous hydrogen-air mixture, *Proc. Combust. Inst.* **30**, 875 (2005).
- [52] A. Konduri, A. Gruber, C. Xu, T. Lu, A. Krisman, M. R. Bothien, and J. H. Chen, Direct numerical simulation of flame stabilization assisted by autoignition in a reheat gas turbine combustor, *Proc. Combust. Inst.* (2018), doi:[10.1016/j.proci.2018.06.084](https://doi.org/10.1016/j.proci.2018.06.084).
- [53] C. A. Kennedy and M. H. Carpenter, Several new numerical methods for compressible shear-layer simulations, *Appl. Numer. Math.* **14**, 397 (1994).
- [54] C. A. Kennedy, M. H. Carpenter, and R. M. Lewis, Low-storage, explicit Runge-Kutta schemes for the compressible Navier-Stokes equations, *Appl. Numer. Math.* **35**, 177 (2000).
- [55] R. Borghi, Turbulent combustion modeling, *Prog. Energy Combust. Sci.* **14**, 245 (1988).
- [56] P. Zhao, L. Wang, and N. Chakraborty, Analysis of the flame-wall interaction in premixed turbulent combustion, *J. Fluid Mech.* **848**, 193 (2018).
- [57] Y. S. Kwon, J. Philip, C. M. de Silva, N. Hutchins, and J. P. Monty, The quiescent core of turbulent channel flow, *J. Fluid Mech.* **751**, 228 (2014).